COMMUNICATIONS IN COMPUTATIONAL PHYSICS
Vol. **5**, No. 2-4, pp. 515-531

Commun. Comput. Phys.
February 2009

Numerical Solution of Partial Differential Equations in Random Domains: An Application to Wind Engineering

Claudio Canuto* and Davide Fransos

Dipartimento di Matematica, Politecnico di Torino, C.so Duca degli Abruzzi 24, 10129 Torino, Italy.

Received 10 October 2007; Accepted (in revised version) 31 December 2007

Available online 1 August 2008

Abstract. An application of recent uncertainty quantification techniques to Wind Engineering is presented. In particular, the study of the effects of small geometric changes in the Sunshine Skyway Bridge deck on its aerodynamic behavior is addressed. This results in the numerical solution of a proper PDE posed in a domain affected by randomness, which is handled through a mapping approach. A non-intrusive Polynomial Chaos expansion allows to transform the stochastic problem into a deterministic one, in which a commercial code is used as a black-box for the solution of a number of Reynolds-Averaged Navier-Stokes simulations. The use of proper Gauss-Patterson nested quadrature formulas with respect to a Truncated Weibull probability density function permits to limit the number of these computationally expensive simulations, though maintaining a sufficient accuracy. Polynomial Chaos approximations, statistical moments and probability density functions of time-independent quantities of interest for the engineering applications are obtained.

AMS subject classifications: 65C20, 65N35

Key words: Uncertainty quantification, stochastic partial differential equations, random domains, mapping approach, polynomial chaos, wind engineering.

1 Introduction

Wind Engineering models incorporate various parameters which are or potentially may be affected by uncertainty; they concern both the fluid-dynamic and the structural components of each model. The study of the wind field has indeed been approached over the years by statistical models based on observation data. On the other hand, until recently,

*Corresponding author. *Email addresses:* `claudio.canuto@polito.it` (C. Canuto), `davide.fransos@polito.it` (D. Fransos)

 ©2009 Global-Science Press

the study of the aerodynamic and aeroelastic behavior of structures has been mostly accomplished by deterministic approaches. Yet, geometric uncertainties may dramatically influence the reliability of the model. For instance, as in Aerospace Engineering [11], random discrepancies between the ideal geometries conceived in the design phase and their actual realization tested in wind tunnels may lead to significant variations in the resulting flow field. The development of efficient tools for the uncertainty quantification of the response of structures is therefore an important task for Wind Engineering.

From the mathematical point of view, geometric uncertainties lead to the formulation of boundary value problems in random domains. As an alternative to expensive Monte-Carlo techniques, the transformation of such problems into deterministic ones by an appropriate change of unknowns allows their discretization by standard numerical methods. Karhunen-Loeve (KL) and Polynomial Chaos (PC) expansions [9, 19] provide the mathematical ground for these transformations. Different methodologies have been explored in the recent literature for handling the randomness of the domain; they include the mapping of each random domain to a reference domain [4, 11, 14, 20], the inclusion of the random domains into a fictitious domain to which the PDE is extended [3], the solution of the deterministic PDEs satisfied by the moments of the variables of interest [10]. In the Wind Engineering applications the number of the random variables is usually fairly small (thus the use of sparse methods is not mandatory). On the other hand, the computational cost of a single simulation on a given realization of the random domain is so high that non-intrusive/collocation methods are practically unavoidable. Within them, the selection of the interpolation/collocation grids is critical to achieve an acceptable balance between cost and accuracy.

This paper is a step of an ongoing project aiming at describing a set of stochastic effects on bridges [6]. Here we isolate a single input random variable related to the bridge deck cross-section (the curvature radius of the lower surface's corners) and we investigate its effects on the statistics of some relevant time-averaged integral quantities of the flow.

We compute the approximate PC with respect to a Truncated Weibull probability density function, and the associated family of nested Gauss-Patterson formulas. They are used in the reconstruction of finite PC expansions from the outputs of a limited number of Reynolds-Averaged Navier-Stokes simulations.

We give an application to the case study of the Sunshine Skyway Bridge deck. Two incident turbulence regimes give rise to two different patterns of the PC expansion. In both cases, sufficiently accurate PC approximations are obtained.

2 Mathematical setting

In order to present the mathematical setting that will be used in the Wind Engineering application, we first consider a linear scalar model, which is representative of some of the relevant features of the subsequent model without being affected by its complications.

Let $(\Omega,\mathcal{F},\mathcal{P})$ be a probability space, where Ω is the state space, $\mathcal{F}$ is the σ-algebra of

the events and $\mathcal{P}$ is the probability measure. For any $\omega\in\Omega$, let $\tilde{D}(\omega)\subseteq D^*\subset\mathbb{R}^d$ be a given bounded domain, whose Lipschitz boundary $\partial\tilde{D}(\omega)$ depends on ω; D^* is a fixed domain. We assume that $\tilde{\Gamma}(\omega)$ depends on ω through the values $y_q=Y_q(\omega)$, $1\leq q\leq Q$, of Q independent random variables with zero mean and unit variance, distributed according to density functions $\rho_q(y_q)$ defined in intervals $I_q\subseteq\mathbb{R}$ and strictly positive in their interiors. Setting

$$y=(y_q)_{1\leq q\leq Q},\quad I=\prod_{q=1}^{Q}I_q,\quad \rho(y)=\prod_{q=1}^{Q}\rho_k(y_q),$$

the random domains $\tilde{D}(\omega)$, $\omega\in\Omega$, can be parametrized by $y\in I$: thus, from now on we will set $D(y)=\tilde{D}(\omega)$ if $y=(Y_1(\omega),\cdots,Y_Q(\omega))$. Similarly, a function $\tilde{u}=\tilde{u}(\tilde{D}(\omega))$ depending on $\tilde{D}(\omega)$ will be denoted by $u(y)$.

Let us fix $y\in I$ and set $D=D(y)$ for shortness. Assume that its boundary $\Gamma=\partial D$ be divided into a non-empty Dirichlet part $\Gamma_{\rm Dir}$ and a complementary Neumann part $\Gamma_{\rm Neu}$. We consider the time-periodic advection-diffusion problem

$$\begin{cases} u_t-\Delta u+\beta\cdot\nabla u=f & \text{in } D, \quad t\in\mathbb{R},\\ u=0 \quad \text{on } \Gamma_{\rm Dir}, \quad \dfrac{\partial u}{\partial n}=0 \quad \text{on } \Gamma_{\rm Neu}, & t\in\mathbb{R},\\ u(t+T)=u(t), & t\in\mathbb{R}. \end{cases} \tag{2.1}$$

Here, $T>0$ is a fixed period, β and f are T-periodic time-dependent functions defined on D^* (hence, independent of y) such that $\beta\in L^\infty(0,T;(W^{1,\infty}(D^*))^d)$ and $f\in L^2(0,T;L^2(D^*))$. We assume that a.e. in time

$$\nabla\cdot\beta=0 \quad \text{in } D \quad \text{and} \quad \beta\cdot n\geq 0 \quad \text{on } \Gamma_{\rm Neu},$$

where n denotes the outward unit normal vector to Γ. Setting

$$H^1_{\rm Dir}(D)=\{v\in D:\ v=0 \text{ on } \Gamma_{\rm Dir}\},$$

the existence and uniqueness of a time-periodic variational solution u satisfying $u\in L^2(0,T;H^1_{\rm Dir}(D))$ and $u_t\in L^2(0,T;(H^1_{\rm Dir}(D))')$ follows from the uniform (in t) continuity and coercivity of the bilinear form

$$a(t;w,v)=\int_D(\nabla w\cdot\nabla v+\beta(t)\cdot\nabla w\, v) \quad \text{in } H^1_{\rm Dir}(D)$$

(see [12], Thm. 6.1). We denote such solution by $u(y)$ and we assume that its dependence on y is sufficiently smooth (see below).

We are interested in computing statistics of *time averages* of functions or functionals derived from $u(y)$: For instance, if $L(y):H^1_{\rm Dir}(D(y))\to\mathbb{R}$ is a linear continuous functional, we consider the variable $\eta:I\to\mathbb{R}$ defined as

$$\eta(y)=\frac{1}{T}\int_0^T L(y)u(t,y)\,dt. \tag{2.2}$$

2.1 The mapping approach

Mapping each problem (2.1) defined in $D(y)$ onto an equivalent problem defined in a fixed domain $\hat{D}$ may help the theoretical analysis of the PC approximation, as well as the computation of statistical quantities. We stress, however, that we invariably solve numerically the problems on the physical domains.

Let $\hat{D}\subset\mathbb{R}^d$ be a bounded domain with Lipschitz boundary $\hat{\Gamma}$ partitioned into a non-empty Dirichlet part $\hat{\Gamma}_{\rm Dir}$ and a complementary Neumann part $\hat{\Gamma}_{\rm Neu}$. For any $y\in I$, let $\gamma(y):\hat{\Gamma}\to\Gamma(y)$ be a smooth invertible mapping, such that $\gamma(y)(\hat{\Gamma}_{\rm Dir})=\Gamma_{\rm Dir}(y)$ and $\gamma(y)(\hat{\Gamma}_{\rm Neu})=\Gamma_{\rm Neu}(y)$. Let us extend $\gamma(y)$ to the interior of $\hat{D}$, getting a mapping $\Phi(y):\overline{\hat{D}}\to\overline{D(y)}$, i.e.,

$$\Phi(\hat{x},y)=x,\quad\text{such that}\quad\Phi(y)|_{\hat{\Gamma}}=\gamma(y).$$

We assume that $\Phi(y)$ is an invertible C^1-mapping in $\overline{\hat{D}}$, such that the determinant $|J_\Phi(\hat{x},y)|$ of its Jacobian matrix $J_\Phi(\hat{x},y)=D_{\hat{x}}\Phi(\hat{x},y)$ satisfies

$$0<c_1\le|J_\Phi(\hat{x},y)|\le c_2<+\infty\qquad\forall\hat{x}\in\hat{D},\tag{2.3}$$

for constants c_1 and c_2 independent of $y\in I$. Let $\Psi(y):\overline{D(y)}\to\overline{\hat{D}}$ be the inverse mapping $\Psi(y)=(\Phi(y))^{-1}$, which enjoys similar properties.

It is easily seen that Problem (2.1) in $D(y)$ is equivalent to the following problem in $\hat{D}$:

$$\begin{cases}\hat{u}_t-\hat{\nabla}\cdot\hat{A}\hat{\nabla}\hat{u}+\hat{\beta}\cdot\hat{\nabla}\hat{u}=\hat{f} & \text{in }\hat{D}, & t\in\mathbb{R},\\ \hat{u}=0\quad\text{on }\hat{\Gamma}_{\rm Dir}, & \dfrac{\partial\hat{u}}{\partial\hat{n}_A}=0\quad\text{on }\hat{\Gamma}_{\rm Neu}, & t\in\mathbb{R},\\ \hat{u}(t+T)=\hat{u}(t), & & t\in\mathbb{R},\end{cases}\tag{2.4}$$

where $\hat{\nabla}$ is the gradient with respect to the variable $\hat{x}$,

$$\hat{A}(\hat{x},y)=|J_\Phi(\hat{x},y)|J_\Psi(x,y)J_\Psi(x,y)^T$$

with

$$x=\Phi(\hat{x},y),\quad\hat{\beta}(\hat{x},t,y)=|J_\Phi(\hat{x},y)|J_\Psi(x,y)\beta(x,t),$$
$$\hat{f}(\hat{x},t,y)=|J_\Phi(\hat{x},y)|f(x,t),\quad\frac{\partial\hat{u}}{\partial\hat{n}_A}=\hat{n}\cdot\hat{A}\hat{\nabla}\hat{u}.$$

The two solutions are related by the identity $u(x,t,y)=\hat{u}(\hat{x},t,y)$.

Under the above assumptions, one has $\|\hat{u}(y)\|_{\hat{X}}\le C$ for all $y\in I$, where

$$\hat{X}=\{\hat{v}\in L^2(0,T;H^1_{\rm Dir}(\hat{D}))\colon\hat{v}_t\in L^2(0,T;(H^1_{\rm Dir}(\hat{D}))')\}$$

equipped with the graph norm. In particular, this implies

$$\hat{u}\in L^2_\rho(I;\hat{X})=\{\hat{v}:I\to\hat{X}\colon\int_I\|\hat{v}(y)\|^2_{\hat{X}}\,\rho(y)\,dy<\infty\}.$$

Furthermore, averages like (2.2) belong to $L^2_\rho(I)=L^2_\rho(I;\mathbb{R})$.

If $\Phi(y)$ depends smoothly upon $y\in I$ in the $C^1(\overline{\hat{D}})$-norm, then the coefficients and the right-hand side which appear in (2.4) depend smoothly upon y in the appropriate norms. In turn, this implies (see [1,3,17] for similar results) that $\hat{u}(y)$ inherits the same degree of smoothness in y as $\Phi(y)$, with respect to the $\hat{X}$-norm.

2.2 Non-intrusive Polynomial Chaos approximations

We now introduce the Polynomial Chaos expansion of such variables as $\hat{u}(y)$ or $\eta(y)$ defined above, as well as certain non-intrusive approximations of them.

Let us assume that, for each $q=1,\cdots,Q$, the space $L^2_\rho(I)$ contains all the algebraic polynomials on I. Then, by the assumptions on the densities $\rho_q(y_q)$, there exists a family of polynomials $\{\varphi_k^{(q)}\}_{k\in\mathbb{N}}$ which is orthonormal with respect to the inner product

$$(u,v)_{\rho_q}=\int_{I_q}u(y_q)v(y_q)\rho_q(y_q)\,dy_q$$

and complete in $L^2_{\rho_q}(I_q)$; in addition, $\deg\varphi_k^{(q)}=k$ for all k. By tensorization, we obtain an orthonormal and complete family $\{\varphi_k\}_{k\in\mathcal{K}}$ of multivariate polynomials in $L^2_\rho(I)$; here, $\mathcal{K}=\mathbb{N}^Q$. Thus, we have the Polynomial Chaos expansions

$$\hat{u}(y)=\sum_{k\in\mathcal{K}}\hat{u}_k\varphi_k(y),\qquad\text{or}\qquad\eta(y)=\sum_{k\in\mathcal{K}}\hat{\eta}_k\varphi_k(y),$$

with $\hat{u}_k=\hat{u}_k(x,t)=(\hat{u},\varphi_k)_\rho\in\hat{X}$, or $\hat{\eta}_k=(\eta,\varphi_k)_\rho\in\mathbb{R}$. With no loss of generality, the subsequent discussion will be focussed on the function $\eta(y)$ only.

In order to obtain easily computable approximations of η, let us introduce M distinct points $y_j\in I$, with $j\in\mathcal{J}_M$ (a set of indices of cardinality M). We assume that there exists an M-dimensional space $S_M=\text{span}\{\varphi_k:k\in\mathcal{K}_M\subset\mathcal{K}\}$ for which the set $\{y_j\}_{j\in\mathcal{J}_M}$ is *unisolvent*, i.e., the matrix $(\varphi_k(y_j))_{k\in\mathcal{K}_M,j\in\mathcal{J}_M}$ is nonsingular. Then, after computing the quantities $\eta(y_j)$, $j\in\mathcal{J}_M$, in a non-intrusive way, i.e., by solving M independent problems (2.1) and applying (2.2), we can approximate η by its interpolant

$$I_M\eta(y)=\sum_{k\in\mathcal{K}_M}\tilde{\eta}_k\varphi_k(y),\qquad\text{defined by}\quad I_M\eta(y_j)=\eta(y_j)\quad\forall j\in\mathcal{J}_M.\tag{2.5}$$

This can be viewed as a particular form of collocation method. An equivalent point of view is as follows: let us choose weights $\rho_j>0$, $j\in\mathcal{J}_M$, and let us define the bilinear form

$$(u,v)_{\rho,M}=\sum_{j\in\mathcal{J}_M}u(y_j)v(y_j)\rho_j,$$

which is indeed an inner product on S_M. Then, $I_M\eta$ satisfies $(I_M\eta,\lambda)_{\rho,M}=(\eta,\lambda)_{\rho,M}$ for all $\lambda\in S_M$, i.e., $I_M\eta$ is the orthogonal projection of η upon S_M with respect to such discrete

inner product, and the coefficients $\tilde{\eta}_k$ are the solutions of the linear system

$$\sum_{k\in\mathcal{K}_M}\tilde{\eta}_k(\varphi_k,\varphi_l)_{\rho,M}=(\eta,\varphi_l)_{\rho,M}\quad\forall l\in\mathcal{K}_M. \tag{2.6}$$

A common way to select the nodes and weights y_j, ρ_j is to require that they define a quadrature formula for the measure $\rho(y)dy$ with sufficiently high polynomial exactness. So we can assume that there exists a nonempty maximal subset $\mathcal{K}'_M\subseteq\mathcal{K}_M$ such that $(\varphi_k,\varphi_l)_{\rho,M}=(\varphi_k,\varphi_l)_\rho=0$ for all $k,l\in\mathcal{K}'_M$, $k\neq l$. Setting

$$S'_M=\text{span}\{\varphi_k\colon k\in\mathcal{K}'_M\}\subseteq S_M,$$

we can define the orthogonal projection P'_M upon S'_M with respect to the discrete inner product, i.e.,

$$P'_M\eta(y)=\sum_{k\in\mathcal{K}'_M}\check{\eta}_k\varphi_k(y),\qquad\text{with}\quad\check{\eta}_k=\frac{(\eta,\varphi_k)_{\rho,M}}{(\varphi_k,\varphi_k)_{\rho,M}}. \tag{2.7}$$

$P'_M\eta$ is again a computable approximation of η, possibly different from $I_M\eta$. The set $\mathcal{K}'_M$ contains the subset

$$\mathcal{K}''_M=\{l\in\mathcal{K}_M\colon(\varphi_k,\varphi_l)_{\rho,M}=0\ \forall k\in\mathcal{K}_M,\ k\neq l\}.$$

The linear system (2.6) has a diagonal block corresponding to $\mathcal{K}''_M$, i.e.,

$$\tilde{\eta}_l=\frac{(\eta,\varphi_l)_{\rho,M}}{(\varphi_l,\varphi_l)_{\rho,M}}=\check{\eta}_l,\qquad\forall l\in\mathcal{K}''_M, \tag{2.8}$$

whereas in general the block corresponding to $\mathcal{K}_M\setminus\mathcal{K}''_M$ is non-diagonal.

The approximation properties of the operators I_M and P'_M as $M\to\infty$ depend on the specific choice of the space S_M and the nodes $\{y_j\}_{j\in\mathcal{J}_M}$.

3 Application and results

The case study of the Sunshine Skyway Bridge (Fig. 1) deck is addressed in this section. Large differences between the time-averaged forces acting on the design deck section (with sharp edges, Fig. 2) and the wind tunnel model (with rounded edges, due to the manufacturing technology) have been observed, both by experimental tests and computational simulations [13, 16].

The aim of the work is to introduce a suitable random variable in order to describe this geometric uncertainty and to apply the techniques of Section 2 to the quantification of its effects on some engineering relevant parameters. Wind tunnel section models can be realized by bending aluminum sheets to replicate a bridge deck segment. This may lead to rounded edges instead of ideal project sharp edges. Rounded edges in the lower surface are considered in the following (Fig. 2). A curvature radius $0.01B<R^*<0.05B$ is studied, where B is the chord of the deck cross section.

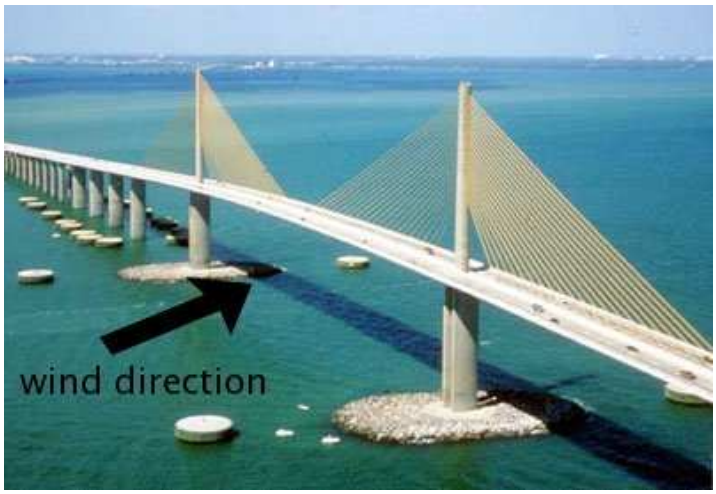

Figure 1: The Sunshine Skyway Bridge (Tampa, Florida).

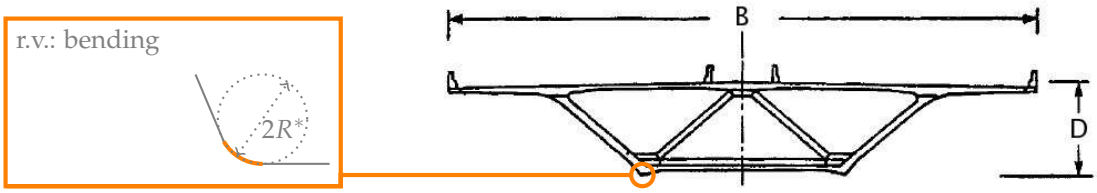

Figure 2: Actual Sunshine Skyway Bridge deck cross section (from [16]) and rounded corner involved by the bending of the aluminum sheet.

3.1 Flow modelling

The turbulent flowfield around the 2D section is modeled by the classical time-dependent Navier-Stokes equations, along with the $k-\omega$ turbulence model, posed in a random domain $D(R^*)$. The Reynolds number is considered to be $Re=UB/\nu=5.76e5$, where U is the incoming flow velocity and ν the kinematic viscosity, accordingly with the experimental setups. Dirichlet conditions on the velocity field and on the turbulence characteristic quantities (k and ω) are imposed at the inlet boundaries. Neumann conditions involving the velocity field and the pressure (null normal component of the stress tensor) as well as the same Dirichlet conditions on k and ω are imposed at the outlet boundaries. No-slip conditions are imposed at the section surface. The values of k and ω can be more easily determined throughout two other quantities to which usually experimental setups refer to, turbulence intensity It and turbulence characteristic length scale Lt. The value $It=0.01$ is fixed for the first, while two different values $Lt=1$ and $Lt=0.001$ will be considered in the following for the second. Impulsive initial conditions are introduced.

Bearing in mind that the non-intrusive approach allows every collocation subproblem to be evaluated on the physical domain (see Section 2), a commercial software can be

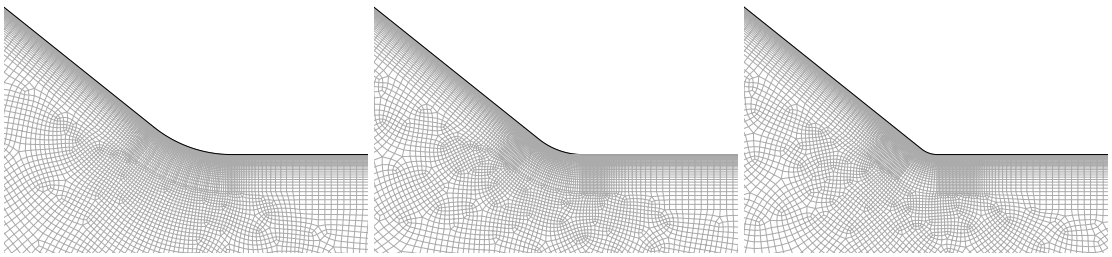

Figure 3: Different realizations of the lower surface corner, from the maximal value $R^*=0.05B$ (on the left) to the minimal value $R^*=0.01B$ (on the right) of the curvature radius R^*.

used as a black-box in order to solve the above equations for every required realization of $D(R^*)$. Some of these realizations are shown in Fig. 3.

The commercial Finite Volume solver Fluent® is used in the following to numerically evaluate the flowfield. A description of the numerical method can be found for instance in [5]. A hybrid quadrilateral/triangular grid is employed. The cell-center values of the variables are interpolated at face locations using a second order Central Difference Scheme for the diffusive terms on all the elements and Quadratic Upwind Interpolation for Convective Kinematics (QUICK) and second-order Upwind Scheme (2UPW) for the convection terms on quadrilateral and triangular cells, respectively. Advancement in time is accomplished by the two-step Backward Differentiation Formulae (BDF) method.

The flowfield is characterized by an unsteady vortex shedding in the wake, along with possible separation and reattachment of the boundary layer on the upper and lower surfaces of the section. A numerical and physical transitory has to be simulated for every domain realization, until a time-periodic behavior is reached. Then, the corresponding flowfield has to be simulated for a sufficient time in order to compute the time statistics of interest for engineering applications, such as time statistics of pointwise (time-averaged pressure coefficient) or integral (Strouhal number, time-averaged forces) parameters.

Computations were carried out on a single Intel Xeon X5355 2.66GHz CPU with 2GB of memory. Every computational grid consists of about 243.000 cells. The timestep needed for an accurate advancement in time is $\Delta t = 0.01$. The transient and periodic parts are then sufficiently covered with 6000 timesteps, thus resulting in about 60 hours of CPU time for each realization.

In this paper, the only parameter of stochastic interest will be R^*. A more complete investigation of the set of uncertain parameters will be presented in [6].

3.2 Polynomial Chaos characterization of time independent quantities

We consider the normalized radius $R=R^*/B$ as our input random variable. Precisely, we introduce a random variable Y which is distributed according to the following probability

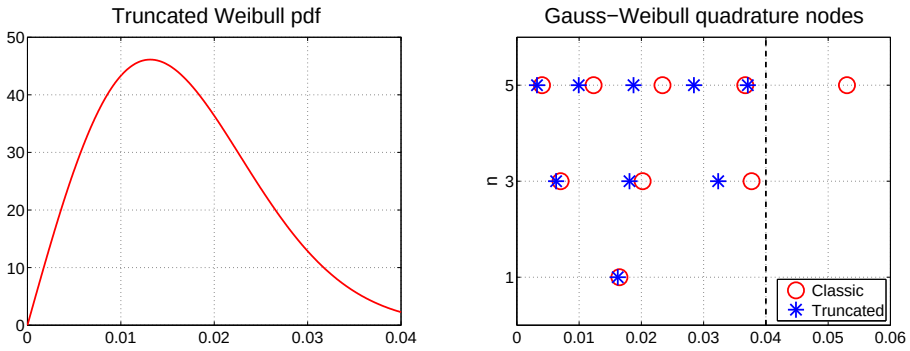

Figure 4: Truncated Weibull probability density function (on the left) and corresponding Gaussian quadrature nodes (on the right). The vertical dashed line confines the interval of truncation.

density function (pdf):

$$\rho(y|\alpha,\beta)=c\beta\alpha^{-\beta}x^{\beta-1}e^{-(x/\alpha)^{\beta}}\chi_{[0,0.04]}(y), \tag{3.1}$$

which is a truncation of the classical Weibull density to the interval $I=[0,0.04]$. The truncation is motivated by the subsequent interest in using collocation nodes only in the interval of variation of R. The parameters are chosen to be $\alpha=0.0186$ and $\beta=2$, whereas c is the normalization coefficient relative to I. The pdf for such a choice of the parameters is plotted in Fig. 4 (on the left). The curvature radius R of the lower surface corners is then assumed to be the random variable $R=0.01+Y$. Its values depend on y as $R(y)=0.01+y$.

A family of orthonormal polynomials $\{\varphi_k(y)\}$, $k\geq 0$, w.r.t. $\rho(y)$ exists, as mentioned in Section 2; the coefficients of the three-term recursive relation, as well as the corresponding n-point Gaussian quadrature formulas can be constructed, following [7]. An example of Gaussian nodes w.r.t. the truncated pdf is shown in Fig. 4 (on the right), compared with the nodes of the Gaussian formula w.r.t. the classical Weibull pdf. Note that already for $n=5$ the rightmost node of the latter formula is outside the interval of interest. The approximation properties of the polynomials $\{\varphi_k(y)\}_{k\geq 0}$ are similar to those of the Jacobi polynomials $\left\{P_k^{(0,1)}(y)\right\}_{k\geq 0}$. In particular, truncation and interpolation yield spectrally accurate approximations of smooth functions (see [2,19]).

However, bearing in mind the cost of a single node evaluation, i.e., about 60 hours, a family of less accurate, but nested, quadrature formulas is indeed preferred when subsequent levels of approximation are required. A family of nested quasi-Gaussian formulas w.r.t. the Truncated Weibull density ρ has been constructed using the classical Patterson algorithm [15], starting from the Gaussian 3-point formula. Such quadrature formulas represent the optimal extension of a n-point rule to a $2n+1$-point one. The $2n+1$-point rule is $3n+1$ precise. The corresponding quadrature nodes are plotted in Fig. 5. The flowfield evaluation is then performed for one set of such quadrature nodes.

Among the output random variables of interest, we first consider the time-averaged Lift Coefficient $\overline{C}_L=\overline{C}_L(R)$ and the Strouhal number $St=St(R)$. The Lift Coefficient C_L

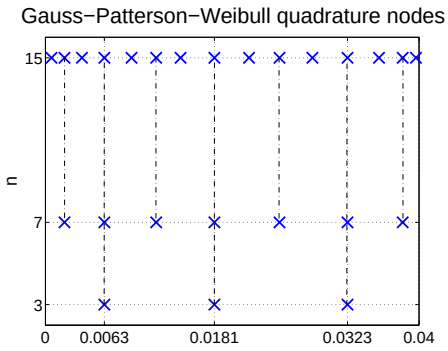

Figure 5: Gauss-Patterson quadrature nodes w.r.t. the Truncated Weibull probability density function.

is defined as the non-dimensional force acting on the bridge deck cross section in the vertical direction and is obtained by integration of the vertical component of the stress tensor

$$\mathrm{T} = -p\mathrm{I} + \frac{1}{Re}\nabla\mathbf{u}$$

along the section's wall Σ:

$$C_L(t) = \frac{1}{\frac{1}{2}\rho U^2 B}\int_\Sigma \mathrm{T}(x,t)\cdot\hat{\mathbf{j}}\, d\sigma, \tag{3.2}$$

where ρ is the density of the fluid, U is the horizontal incident velocity and $\hat{\mathbf{j}}$ is the unit vector in the vertical direction.

The Strouhal number is defined as $St = f_s D/U$, where f_s is the main frequency of the vortex shedding. The latter can be identified from C_L by a frequency analysis, defining it as the frequency corresponding to the maximum of the power spectrum of C_L.

The values of the random variable $\overline{C_L}(R)$ are given by $\overline{C_L}(R(y))$, $y \in [0,0.04]$. For simplicity we will denote by $\overline{C_L}(y)$ the function $y \mapsto \overline{C_L}(R(y))$. Similarly, $St(y)$ will denote the function $y \mapsto St(R(y))$. We now resort to a Polynomial Chaos expansion of these variables, i.e., we write

$$\overline{C}_L(y) = \sum_{k=0}^{\infty} \hat{c}_k \varphi_k(y), \qquad St(y) = \sum_{k=0}^{\infty} \hat{s}_k \varphi_k(y). \tag{3.3}$$

Note that $\overline{C}_L$ and St are obtained by time-averages, i.e., they do not depend on time. A Polynomial Chaos description of the time dependent variables is therefore not needed for the aim of the present work.

We compute the values of $\overline{C}_L$ and St at the nodes of one of the Gauss-Patterson formulas mentioned above. Let $M = N+1$ be the number of nodes, i.e., with the notation of Section 2, we set $\mathcal{K}_M = \mathcal{K}_{N+1} = \{0,\cdots,N\}$. Then, we replace (3.3) by their interpolants at

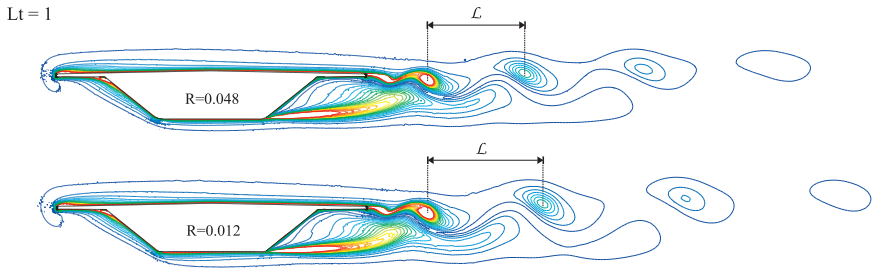

Figure 6: Physics of the flow at $Lt=1$. Vortical structures in the wake.

these nodes, i.e., we compute

$$I_{N+1}\overline{C}_L(y)=\sum_{k=0}^{N}\tilde{c}_k\varphi_k(y),\qquad I_{N+1}St(y)=\sum_{k=0}^{N}\tilde{s}_k\varphi_k(y),\tag{3.4}$$

as introduced in (2.5). Let $2P=\frac{3}{2}N+1$ (which is always an even integer, since N is twice an odd integer) be the order of precision of the $N+1$-point quadrature formula; then, let $\mathcal{K}'_{N+1}=\{0,\cdots,P\}$. Approximate truncated Polynomial Chaoses of order P can be defined by the orthogonal projection P'_{N+1} with respect to the discrete scalar product (see (2.7)) as

$$P'_{N+1}\overline{C}_L(y)=\sum_{k=0}^{P}\check{c}_k\varphi_k(y),\qquad P'_{N+1}St(y)=\sum_{k=0}^{P}\check{s}_k\varphi_k(y).\tag{3.5}$$

At last, we have $\mathcal{K}''_{N+1}=\{0,\cdots,L\}$, with $L=2P-N=\frac{1}{2}N+1$, i.e., $\tilde{c}_l=\check{c}_l$, $\tilde{s}_l=\check{s}_l$, for $0\leq l\leq L$.

3.3 High incoming turbulence length scale

The flowfield around the bridge deck cross section shows slightly different characteristics at varying R in the $Lt=1$ case, as shown in Fig. 6. Vortices are shed from the upper surface only, for both large and small corner curvature radius. The distance $\mathcal{L}$ between the vortices' centers is proportional to f_s, i.e., $St\propto 1/\mathcal{L}$. For larger R this distance decreases, thus leading to a higher St.

A regular decay of about 30% takes place for the computed time-averaged lift coefficient $\overline{C}_L$, when passing from $R=0.012$ to $R=0.048$ (Fig. 7, on the left), making an analysis of these variations of great interest for Engineering. Polynomial Chaos approximations for $N=6$ are shown in the same figure, concerning both the interpolant $I_7\overline{C_L}\in\mathbb{P}_6(I)$ and the projection $P'_7\overline{C_L}\in\mathbb{P}_5(I)$. The overall dependence on R is smooth, although small high-frequency oscillations are present, probably due to model and numerical errors in the evaluations of the flowfields. This is reflected by the behavior of the Polynomial Chaos coefficients, reported in Fig. 7, on the right: the first four coefficients decay at an exponential rate, whereas the last ones indicate the presence of non-negligible high-frequency components.

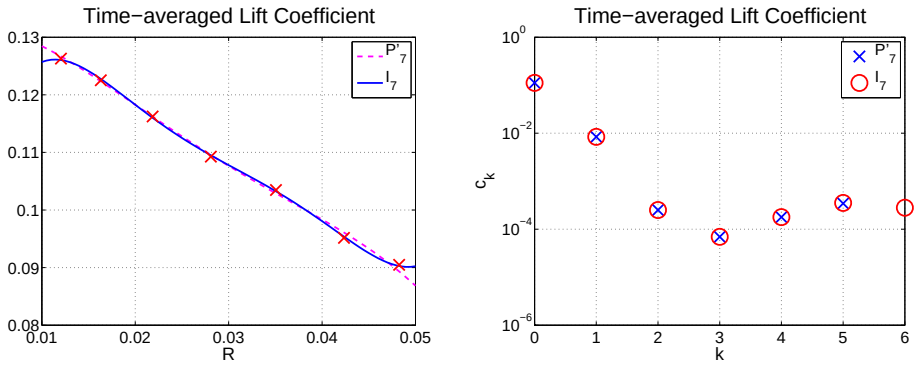

Figure 7: Time-averaged lift coefficient $\overline{C}_L$ at $Lt=1$. PC approximations $I_7\overline{C}_L$ and $P_7'\overline{C}_L$ (left) and their coefficients $\tilde{c}_k$ (circles) and $\check{c}_k$ (crosses) (right).

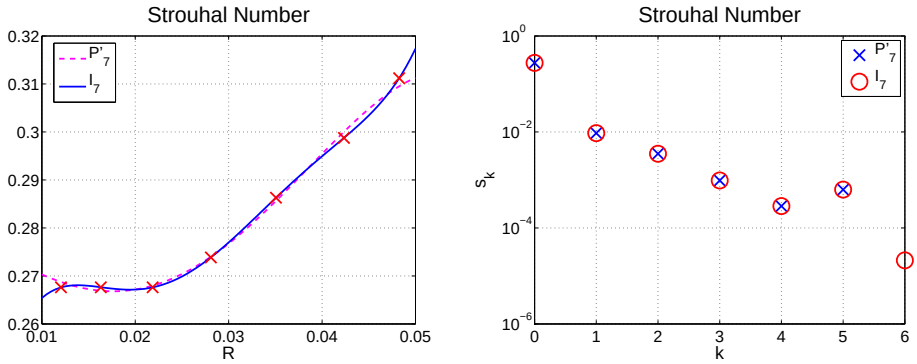

Figure 8: Strouhal number St at $Lt=1$. PC approximations I_7St and $P_7'St$ (left) and their coefficients $\tilde{s}_k$ (circles) and $\check{s}_k$ (crosses) (right).

Similarly, the Strouhal number increases of about 20% from the smallest considered radius to the highest (Fig. 8, on the left). High frequency oscillations are still present (although less pronounced than for the previous quantity), as evidenced by the values of the coefficients of the higher order terms (Fig. 8, on the right).

Mapping the physical domain, or at least a portion of it, on a reference domain is essential in the case of physical space dependent quantities, such as the time-averaged pressure coefficient $\overline{Cp}=2(\overline{p}-p_\infty)/qU^2$. For instance, the lower surface of the bridge deck cross section in the case $R=0.05$ is chosen as reference frame in the following. Mean and variance for the time-averaged Cp on the lower surface (actually a curve) are shown in Fig. 9. Note that the abscissa s/B is a spatial parametrization of this curve, not a random variable.

Finally, the probability density function of some quantity of interest can be obtained from the Polynomial Chaos expansion. One possible way to accomplish this goal is the simulation technique: a set of realizations of the random variables Y_i is generated using an appropriate method. Then a statistical density for the corresponding values of the PC

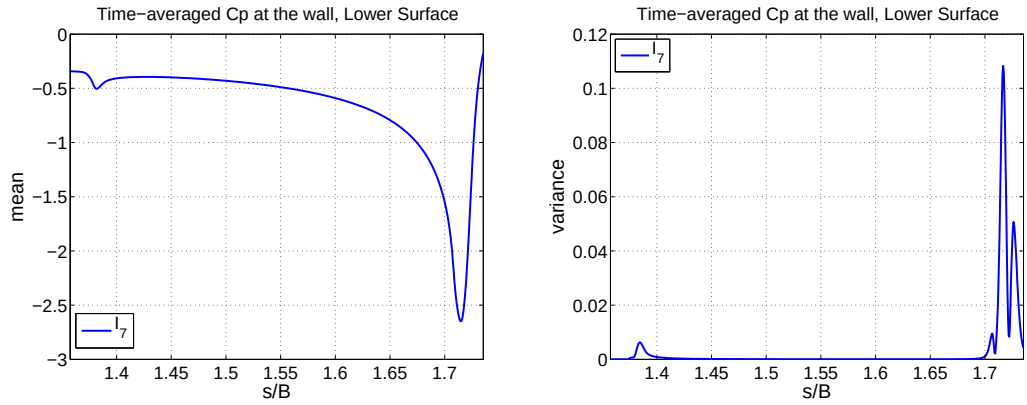

Figure 9: Time-averaged pressure coefficient $\overline{Cp}$ at $Lt=1$. Mean (left) and variance (right) obtained by the Polynomial Chaos interpolation $I_7\overline{Cp}$ on a reference lower surface.

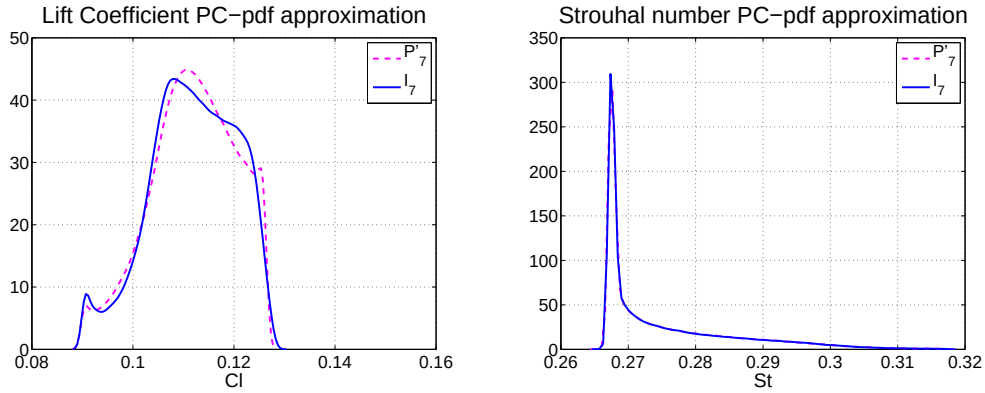

Figure 10: Probability Density Functions approximation at $Lt=1$ with $N+1=7$. Time-averaged Lift Coefficient $\overline{C}_L$ (left) and Strouhal number St (right).

expansion is estimated. In the case of the Truncated Weibull random variables, a rejection method is applied in order to accomplish the random number generation. The resulting pdfs for the Strouhal number and the Lift Coefficient are plotted in Fig. 10.

3.4 Low incoming turbulence length scale

Two completely different flow regimes are put in evidence in the $Lt=0.001$ case. Separation of the boundary layer early occurs at the lower surface for small values of R, no reattachment is present and a large wake is shown. On the contrary, separation does not take place at all for large curvature, thus a thin wake with smaller but more frequent vortices is present. Vortices are shed from both the upper and lower surfaces, but when separation at the lower surface occurs, the characteristic size of this vortices is much greater, leading to a wider wake and a lower St (about one half).

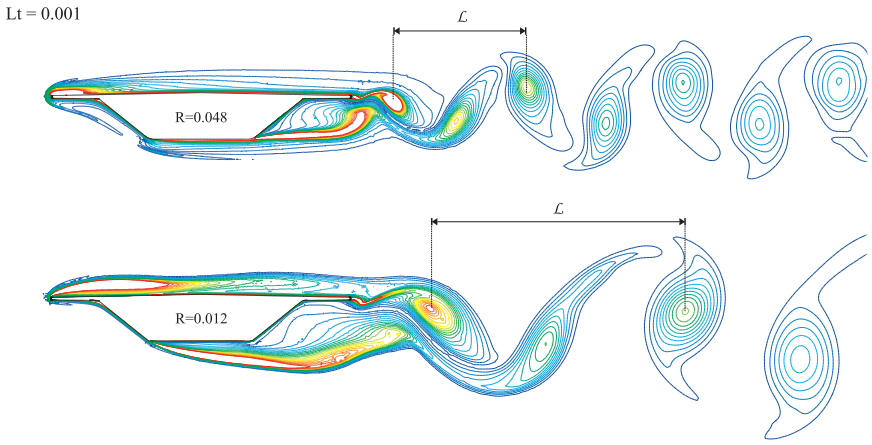

Figure 11: Physics of the flow at $Lt=1$. Vortical structures in the wake.

In terms of lift coefficient, the two flow regimes appear as two ranges in which C_L is almost constant. Between the two ranges, a discontinuity seems to appear. If a steep gradient is present, it should be searched to a smaller scale in terms of differences of R. The apparent discontinuity causes a classical Gibbs phenomenon to appear in the Polynomial Chaos projection $P'_{15}\overline{C}_L \in \mathbb{P}_{11}(I)$, as plotted in Fig. 12 (on the left). Poor convergence of the Polynomial Chaos is evidenced by the slow decay of the PC coefficient, which are shown in Fig. 13 (on the left). Smarter techniques should be employed in this case in order to handle the non-regularity of the stochastic solution. An interesting possibility is the use of adaptive methods, such as the Multi-Element generalized Polynomial Chaos introduced in [18]. An application of adaptive methods to the Skyway Bridge problem with two input random variables will be presented in [6].

In this paper, we present a post-processing discontinuity reconstruction approach (see [8] for different approaches and more references on the argument). The time-averaged Lift Coefficient $\overline{C}_L(y)$ is expressed as the sum of a regular function $G(y)$, which will be expanded in terms of Polynomial Chaos, and a known piecewise linear function:

$$\overline{C}_L(y) = G(y) + Heavyside(y-y_{disc})(p_0+p_1(y-y_{disc})), \tag{3.6}$$

where the parameters p_0 and p_1 are evaluated through an optimization process, in order to maximize the rate of decay of the PC coefficients $\breve{g}_k$ of $P'_{15}G \in \mathbb{P}_{11}(I)$. Precisely, for any choice of p_0 and p_1, the coefficients' decay is least-square fitted by the law

$$|\breve{g}_k| \sim \lambda k^{-\mu},$$

yielding $\lambda=\lambda(p_0,p_1)$ and $\mu=\mu(p_0,p_1)$. The optimal values of p_0 and p_1 are then obtained as $(p_0,p_1)=\text{argmax}(\mu(p_0,p_1))$. The corresponding approximation of the data shows the elimination of the Gibbs phenomenon, as depicted in Fig. 12 (on the right), again for the choice $N=14$. The decay of the approximate PC coefficients of the regular part results to

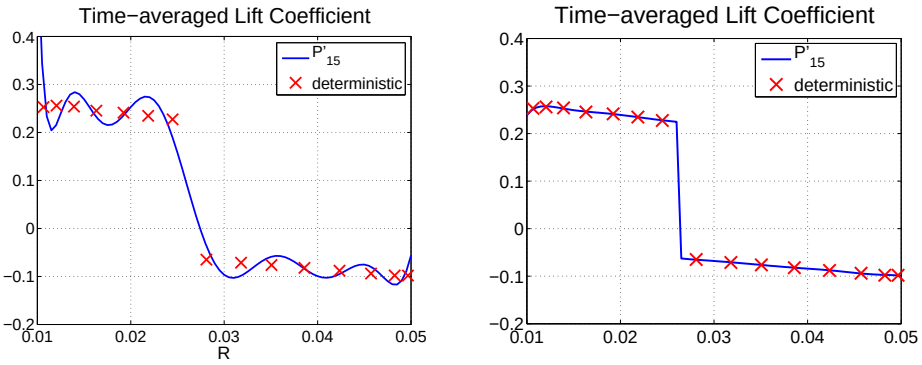

Figure 12: Time-averaged lift coefficient at $Lt=0.001$. PC approximation (left) and PC approximation with discontinuity tracking (right).

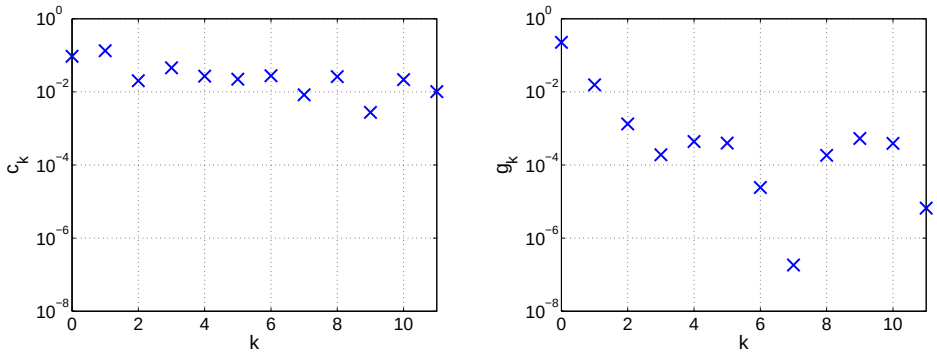

Figure 13: Time-averaged lift coefficient at $Lt=0.001$. PC coefficients of $P'_{15}\overline{C}_L$ (left) and of $P'_{15}G$ (right).

be much faster, as shown in Fig. 13 (on the right). Once these coefficients are computed, statistical quantities of $\overline{C}_L$ can be obtained from (3.6) in a straightforward manner. A similar approach can be applied to derive statistics of the Strouhal number St.

4 Conclusion

An application of generalized Polynomial Chaos techniques to a complex Wind Engineering problem is given in the paper. Randomness in the geometry of a bridge deck section generates uncertainty in the aerodynamic parameters of the section itself; among them, the Strouhal number and the time-averaged Lift Coefficient have been investigated. Gauss-Patterson nested quadrature rules have been employed in order to obtain subsequent levels of approximation. Two different inflow conditions have been considered. A smooth dependence on the input random variable has been shown in the first case, and an accurate gPC representation on the parameters of interest has been achieved. A shock has been observed in the second case, and a shock-subtraction approach has been

successfully employed to overcome the Gibbs phenomenon appearing from a naive approach; once again, a sufficiently accurate chaos representation has been obtained. The investigation of the combined effects of uncertainty in both the geometry and the inflow conditions is planned for future research. The complexity of the dependency of the random output on the two different input random variables suggests the use of adaptive techniques, such as Multi Element generalized Polynomial Chaos. A complete analysis of the problem and an adaptive solution method will be given in [6].

Acknowledgments

The authors would like to thank Prof. L. Bruno (Politecnico di Torino) for his continuos support in understanding and simulating the physics of the aerodynamic phenomena discussed in the paper. The authors wish also to thank Prof. F. Ricciardelli (University of Reggio Calabria) and Dr. C. Mannini (University of Florence) for kindly providing the geometrical properties of the Sunshine Skyway Bridge and the wind-tunnel set-up data. Further thanks go to Dr. S. Khris (Optiflow Company) and Prof. G. Monegato (Politecnico di Torino) for helpful discussions about the topics of the paper.

References

[1] I. Babuška, F. Nobile, and R. Tempone. A stochastic collocation method for elliptic partial differential equations with random input data. *SIAM J. Numer. Anal.*, 45(3):1005–1034, 2007.
[2] C. Canuto, M. Y. Hussaini, A. Quarteroni, and T. A. Zang. *Spectral Methods. Fundamentals in Single Domains*. Scientific Computation. Springer-Verlag, Berlin, 2006.
[3] C. Canuto and T. Kozubek. A fictitious domain approach to the numerical solution of pdes in stochastic domains. *Numerische Mathematik*, 107(2):257–293, 2007.
[4] C. Chauviere, J. S. Hesthaven, and L. C. Wilcox. Efficient computation of rcs from scatterers of uncertain shapes. *IEEE Transactions on Antennas and Propagation*, 55(5):1–12, 2007.
[5] J. H. Ferziger and M. Peric. *Computational Methods for Fluid Dynamics*. Springer, Berlin, 2002.
[6] D. Fransos. Deterministic and stochastic numerical models for wind engineering. *PhD Thesis*, In preparation.
[7] W. Gautschi. *Orthogonal Polynomials: Computation and Approximation*. Numerical Mathematics and Scientific Computation. Oxford University Press, New York, 2004.
[8] A. Gelb and E. Tadmor. Detection of edges in spectral data. *Appl. Comput. Harmon. Anal.*, 7(1):101–135, 1999.
[9] R. G. Ghanem and P. D. Spanos. *Stochastic Finite Elements: A Spectral Approach*. Springer-Verlag, New York, 1991.
[10] H. Harbrecht, R. Schneider, and C. Schwab. Sparse second moment analysis for elliptic problems in stochastic domains. *Preprint No. 304, Universitat Bonn*, 2006.
[11] S. Hosden, R.W. Walters, and R. Perez. A non-intrusive polynomial chaos method for uncertainty propagation in CFD simulations. *AIAA*, (0891), 2006.
[12] J.-L. Lions and E. Magenes. *Problèmes aux Limites Non Homogènes et Applications*. Dunod, Paris, 1968.

[13] C. Mannini. Flutter vulnerability assessment of flexible bridges. Ph.D. thesis, University of Florence - Technische Universität Carolo-Wilhelmina zu Braunschweig, 2006.
[14] L. Mathelin, M. Y. Hussaini, and T. A. Zang. Stochastic approaches to uncertainty quantification in cfd simulations. *Numerical Algorithms*, 38:209–236, 2005.
[15] T. N. L. Patterson. The optimum addition of points to quadrature formulae. *Math. Comp. 22 (1968), 847–856; addendum, ibid.*, 22(104, loose microfiche supp.):C1–C11, 1968.
[16] F. Ricciardelli and H. Hangan. Pressure distribution and aerodynamic forces on stationary box bridge sections. *Wind and Structures*, 4(5):399–412, 2001.
[17] R. A. Todor and C. Schwab. Convergence rates for sparse chaos approximations of elliptic problems with stochastic coefficients. *IMA J. Numer. Anal.*, 27(2):232–261, 2007.
[18] X. Wan and G. Em Karniadakis. Multi-element generalized polynomial chaos for arbitrary probability measures. *SIAM J. Sci. Comput.*, 28(3):901–928 (electronic), 2006.
[19] D. Xiu and G. Em Karniadakis. The Wiener-Askey polynomial chaos for stochastic differential equations. *SIAM J. Sci. Comput.*, 24(2):619–644 (electronic), 2002.
[20] D. Xiu and D. M. Tartakovsky. Numerical methods for differential equations in random domains. *SIAM J. Sci. Comput.*, 28(3):1167–1185 (electronic), 2006.